PARTIAL HINGE DETAILING TO IMPROVE CATENARY ACTION OF REINFORCED CONCRETE FRAMES

Yu Jun[*1] and Tan Kang Hai[1]

[1]*School of Civil & Environmental Engineering, Nanyang Technological University, Singapore*

Abstract

Progressive collapse resistance of buildings can be evaluated by introducing a middle column removal scenario to mobilize alternate load paths (ALP). Catenary action, one of ALPs, uses tensile force throughout beams to balance external loads applied onto structures. To this end, large deflections and rotations of beams must be achieved. Due to the tensile mechanism, the continuity of longitudinal steel reinforcement becomes critical. In this paper, the development of catenary action of two reinforced concrete (RC) frames is presented in detail. Both specimens consisted of two one-bay beams, one middle joint, two side columns and two beam extensions. One frame was designed with conventional non-seismic detailing in accordance with ACI 318-05. To avoid any possible failure at the joint panels and to increase the rotation capacities of beams, detailing of the second frame was improved by designing partial hinges in the beams at one beam depth away from the joint interfaces. The hinges were constructed by bending down one top bar and then leveling it at the bottom bar layer, and bending up one bottom bar and then leveling it to the top bar layer. Test results on the specimen with conventional detailing show that catenary action could be mobilized successfully but failed to significantly increase structural resistance due to excessively premature fracture of top bars at the side joint interfaces. In contrast, the presence of partial hinges in the second frame enabled catenary action to significantly enhance structural resistance, with more than twice the capacity of compressive arch action. This is because that the in-built hinges helped the beams rotate easily without causing premature bar fracture at the initial rotation stage.

***Key words**: Progressive collapse, Catenary action, Reinforced concrete frames, Partial hinges, Rotation capacity*

1. Introduction

A few quasi-static tests were conducted to demonstrate the structural behavior of reinforced concrete sub-assemblages with different detailing rules under a column removal scenario [1-4]. Besides, more systematic tests on RC sub-assemblage behavior subjected to a column removal scenario were carried out [5, 6]. All the foregoing test results indicated that with adequate lateral restraints and increasing beam deflections, both compressive arch action and catenary action can be sequentially mobilized on top of conventional flexural action (or beam action). The test on a one-third scaled, four-bay and three-story RC frame under a ground-story column removal scenario [7] showed that the ultimate structural resistance of the frame was significantly enhanced by catenary action. All the tests indicated that the failure (such as severe concrete crushing, cracking and bar fracture) was mainly concentrated on the beam-column connections, which were located near the joint interfaces.

Sub-assemblage tests were unable to show the structural behavior of two joints and two columns adjacent to a removed column. Moreover, in sub-assemblage tests, the restraints at the ends of beams are typically strengthened so that the beams show good rotation capacity. However, in the latest UFC 4-23-03, the ties are not suggested to be placed within beams or just above beams because the guideline writers are concerned with the inability of tensile bars

in beams to provide tensile force under large rotations. As a result, it is imperative to experimentally demonstrate more realistic frame behavior under column loss scenarios. This study is also conducted to see if the concern expressed in UFC 4-023-03 is justified.

In this paper, the test results of two one-half scaled RC frames subjected to a column removal scenario will be demonstrated. One specimen was designed with conventional non-seismic detailing in accordance with ACI 318-05, and the other with partial hinges in the beams at one beam depth away from the joint interfaces to improve rotation capacity of beam-column connections and catenary action.

2. Specimen design

Fig. 1 shows a change of the bending moment diagram of a typical frame due to the removal of a middle column based on linear elastic analysis. After the column removal, the bending moment near the middle joint at the center of a two-bay beam AB changes sign, and the bending moments at side joints A and B increase significantly. All these changes may not be considered in conventional gravity-dominant design. Therefore, the beam-column frame above the removed column becomes a critical structural element in the entire perimeter frame. However, the frame will endeavor to balance the amplified gravity loads via different alternate load paths prior to any possible collapse. To more realistically demonstrate the structural mechanisms of the critical element, a beam-column frame that consists of a two-bay beam, two beam extensions, two side columns and one middle joint was extracted at the locations of contra-flexural points of bending moments.

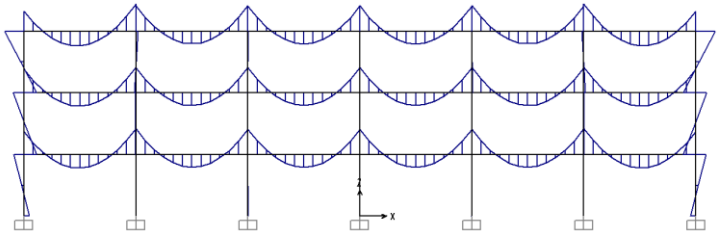

(a) Before the removal of a middle column

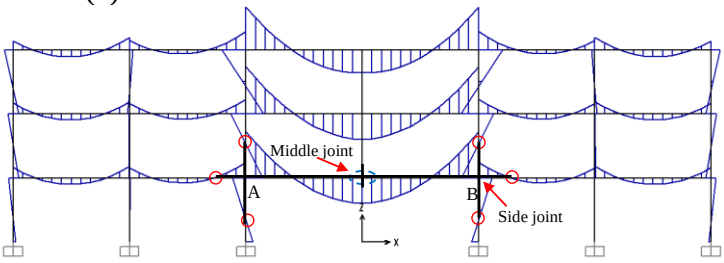

(b) After the removal of a middle column

Fig. 1: Bending moment diagram of a frame

Frame specimens were designed based on the sub-assemblage tests [3, 6]. During the sub-assemblage tests, the effects of the bottom reinforcement ratio (BRR) and top reinforcement ratio (TRR) in the middle joint region and the beam span-to-depth ratio (L/h) on the structural behavior were already studied. Therefore, in the frame tests, these parameters remained constant and the research interests were focused on the effects of specimen detailing on structural behavior. Due to symmetry, the detailing of one half of specimens F-CD and F-PH is demonstrated in Fig. 2(a) and (b), respectively. “CD” denotes conventional detailing and “PH” stands for partial hinge. The BRR of specimens F-CD and F-PH were 0.82% and 0.90%, respectively, but their TRRs remained the same, at 1.24%. “T13” indicates longitudinal hot-rolled deformed bars with a high nominal yield strength of 460 MPa and a nominal diameter of 13 mm. “R6” denotes stirrups with a low nominal yield strength of 250 MPa and a nominal diameter of 6 mm. The center-to-center spacing of

stirrups was 100 mm throughout the whole beam and 200 mm in the columns of specimen F-CD. Except partial hinge regions, which were within 500 mm from the respective joint interface, the arrangement of stirrups in specimen F-PH was identical to that of specimen F-CD. In the partial hinge regions, one top T13 bar and one bottom T13 bar were bent down and up, respectively, at 125 mm away from the adjoining joint interface. Finally, the two bars respectively leveled off at the bottom and top reinforcement layers, making the center of the partial hinge at 250 mm away from the adjoining joint interface, as shown in Fig. 2(b).

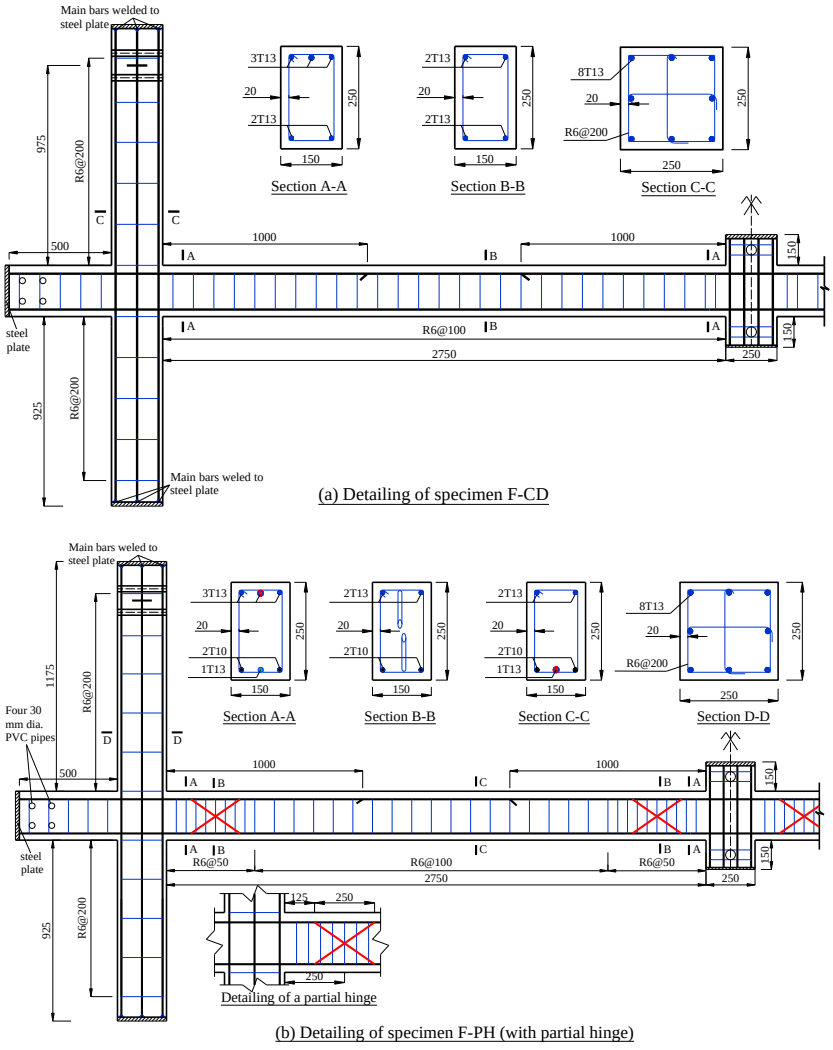

Fig. 2: Detailing of two frame specimens

2. Test set-up

Theoretically, all contra-flexural points in Fig. 1(b) should be replaced by pins in laboratory tests. However, the pins at the top of two side columns are unlikely to transfer vertical loads upwards and column axial deformations are negligible, so finally two horizontal pin-pin connections were used atop two side columns, representing the inter-story restraints in the context of a multi-story building. The vertical loads are mainly transferred to the ground through two side columns. Therefore, the restraints at the ends of two beam extensions are also simplified into pin-pin connections, representing the axial restraints from surrounding structures to the frame. The simplified boundary conditions are illustrated in Fig. 3.

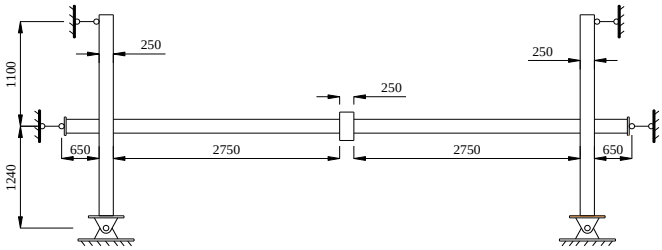

Fig. 3: Simplified boundary conditions

Fig. 4 shows the test set-up for the frame specimens. The top ends of two columns were respectively anchored to a reaction wall and a steel A-frame via a horizontal pin-pin connection. The bottom ends of two columns were respectively supported by a pin connection seated above the ground. The beam extensions were respectively anchored into the reaction wall and the steel A-frame through a horizontal pin-pin connection as well. A tension/compression load cell was installed in each pin-pin connection, so that the corresponding horizontal reaction forces could be measured. A load pin was installed in each bottom pin support, and the load pin could measure the horizontal forces that were transferred into the supports. A concentrated load was then applied at the top of a middle joint through a hydraulic actuator reacting against a steel portal frame. The load was imposed with displacement control at a rate of 0.1 mm/sec until a specimen failed. Two smaller transverse frames were installed on both sides of the middle joint to prevent out-of-plane movement of the slender specimens. Moreover, a rotational restraint was installed at the middle joint position to prevent joint rotation due to asymmetric damage of concrete or fracture of reinforcing bars at either side of the middle joint.

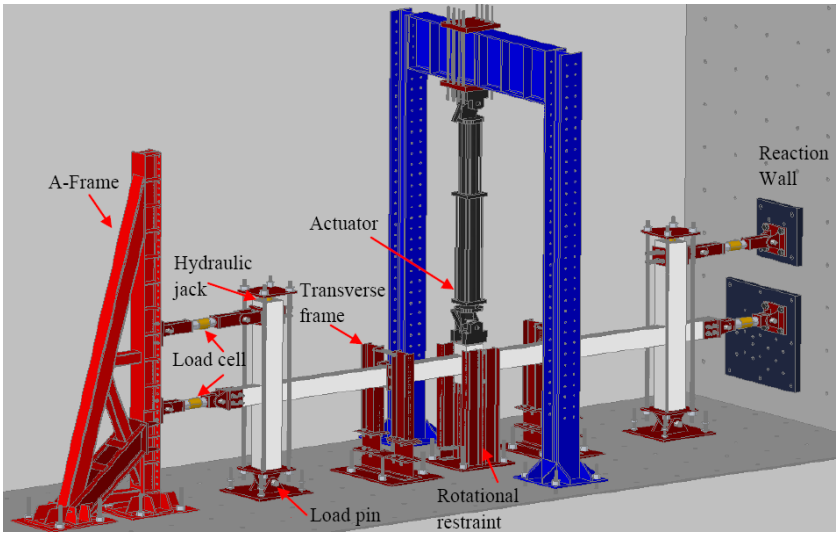

Fig. 4: Test set-up

To consider the effect of column axial force on the behavior of frames and side joints, a hydraulic jack was installed at the top of each side column to apply a constant axial load along the side columns. For each test, the axial stress was $0.6f_c'$ and $0.4f_c'$ at the side columns towards the reaction wall and the A-frame, respectively. The axial load was achieved by using four high-strength steel rods that connected a top steel plate and the bottom pin support. When a hydraulic jack was pumped to apply a force, the top steel plate tended to move upwards but was pulled in by the four steel rods. As a result, the four steel rods were in tension to balance the compression force applied on a side column. Since the hydraulic jack, the four rods, the top and bottom steel plates could form a self-equilibrium system, the applied load would not affect the readings of load cells and load pins.

3. Experimental results

3.1 Material properties

Material tests were conducted according to ASTM specifications to obtain the representative strengths of concrete and steel reinforcement used in frame specimens. The tests included tensile tests for steel reinforcement, compressive cylinder and split-cylinder tests for concrete. Concrete cylinders were tested after 28 days and during the period of frame tests. The material properties of concrete and steel reinforcement are listed in Tables 1 and 2, respectively. Note that the fracture strain of reinforcement corresponds to its tensile strength.

Table 1: Material properties of concrete

Specimen	Compressive strength f_c'(MPa)	Elastic modulus E_c (MPa)	Strain ε_c (μ) at f_c'	Tensile strength f_t (MPa)
F-CD	29.69	25473	2436	3.34
F-PH	27.54	22859	2302	2.15

Table 2: Material properties of steel reinforcement

Rebar type	Nominal diameter (mm)	Yield strength f_y (MPa)	Elastic Modulus E_s (MPa)	Strain at the start of hardening ε_{sh} (%)	Tensile strength f_u (MPa)	Ultimate strain ε_u (%)
R6	6	442	209397	--	513	--
T10	10	520	187090	4.12	595	13.70
T13	13	488	170125	2.86	586	11.00

3.2 Load-deflection history

The frame tests were conducted by increasing the middle joint displacement (MJD) until the complete failure of each specimen. During the test, the horizontal reaction forces at each side were measured by two load cells and one load pin, as shown in Fig. 4. The total horizontal reaction to the two-bay beam is the summation of these forces. Moreover, the axial force vs. MJD relationship is always identical to the total horizontal reaction vs. MJD relationship[8].

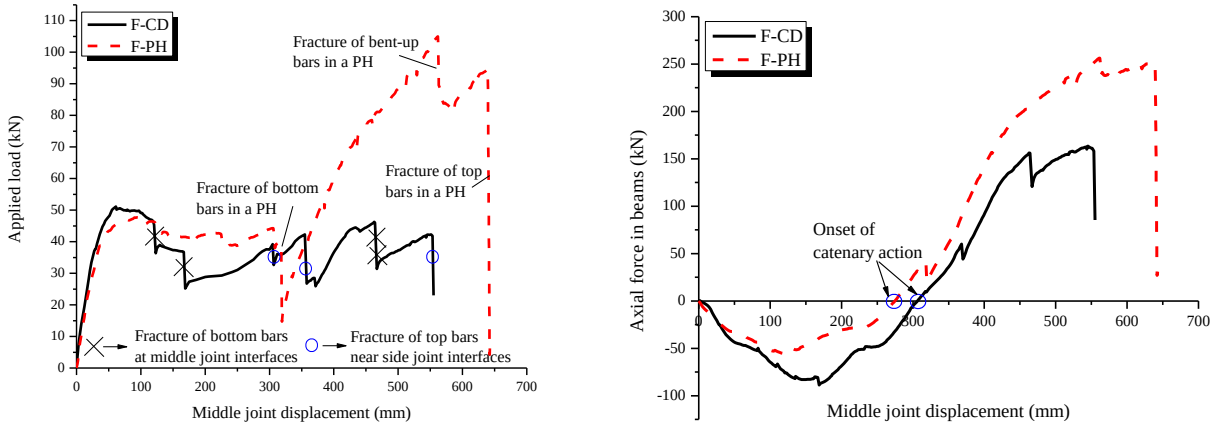

(a) Applied loads (b) Axial forces

Fig. 5: Load-deflection history of two frame specimens

Figs. 5(a) and (b) show the applied load-MJD and axial force-MJD relationships, respectively. Each sudden reduction of applied load resulted from the fracture of reinforcing bars. Fig. 5(b) indicates that both CAA (associated with axial compression in beams) and catenary action (associated with axial tension in beams) were sequentially mobilized.

However, due to consecutive bar fractures, catenary action failed to increase structural resistance of specimen F-CD beyond its CAA capacity, as shown in Fig. 5(a). On the contrary, catenary action significantly enhanced structural resistance of specimen F-PH.

Table 3 summarizes the critical structural resistance, axial force and MJDs in the load-deflection histories for two specimens. It can be seen that the maximum resistance due to catenary action of F-PH was around 2.2 times its CAA capacity. Moreover, both specimens changed from CAA to catenary action at a MJD slightly greater than one beam depth. Finally, compared with specimen F-PH, the early fracture of bars in specimen F-CD reduced deformation capacity and beam axial tension, resulting in a smaller catenary action capacity.

Table 3: Summary of test results

Specimen	Compressive arch action capacity P_{CAA} (kN)	MJD at P_{CAA} (mm)	Max. axial compression $N_{c,max}$ (kN)	MJD at onset of catenary action (mm)	Max. resistance of catenary action P_{CTA} (kN)	MJD at P_{CTA} (mm)	Max. axial tension $N_{t,max}$ (kN)
F-CD	51.10	61.4	-88.87	306.5	46.27	462.8	163.42
F-PH	47.77	94.8	-55.97	274.8	105.04	562.1	256.43

3.3 Crack patterns and failure modes

Fig. 6 shows the local failure modes at the beam-column connections of specimen F-CD. Throughout the entire load-deflection history, the failures, including large cracking, severe concrete crushing and spalling as well as bar fracture, were mainly concentrated at the beam-column connections so as to achieve large rotations of beams. F-CD eventually failed by fracture of the top bars near a side joint interface, as indicated in Fig. 6(c). At catenary action stage, cracks spread over the whole two-bay beam. However, there were nearly no cracks at the two side columns, except a few hairline flexural cracks at the joint-column interfaces due to bending moments and hairline inclined cracks at the joint panels due to shear, as shown in Fig. 6(a) and (c). This indicates that the shear stress at the side joint panels was very small.

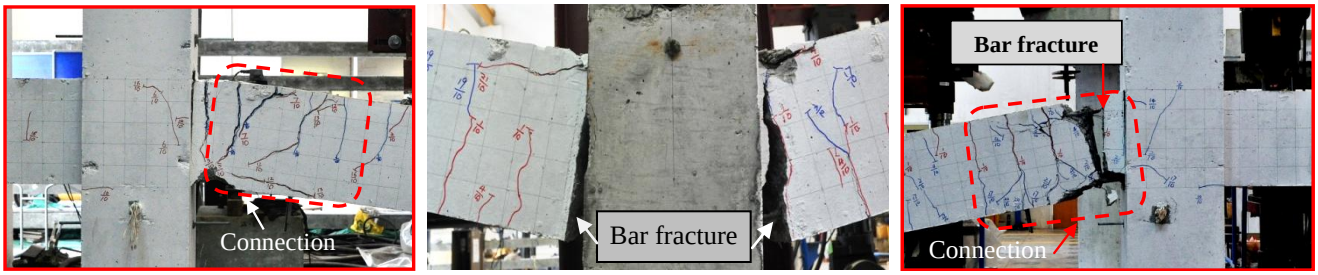

(a) Side joint connected to Reaction Wall

(b) Middle joint

(c) Side joint connected to A-Frame

Fig. 6: Failure modes of specimen F-CD

Since the failure was mainly concentrated on the beam-column connections, a beam segment connected to the middle joint and a side joint were selected to demonstrate the crack patterns of specimen F-PH at different stages in the load-deflection history, as indicated by points A, B, C and D in Fig. 7. Points A and B were in CAA stage, and points C and D were in catenary action stage. Moreover, point D corresponds to the failure mode. It can be found that at stages A and B, only flexural cracks were observed. With further increasing MJD to stage C, flexural cracks widened up within the partial hinges and concrete crushing occurred. At stage D (i.e. end of the test), extensive cracks and large separation of concrete due to fracture of bars occurred at the partial hinge connected to the middle joint. In addition, the large axial tension caused a crack penetrating a section in the beam extension. However, there was only one shear crack at the side joint panel, indicating a small shear stress.

A comparison of crack patterns shown in Figs. (6) and (7) indicates that due to the presence of partial hinges, severe local failure including concrete crushing and wide cracks shifted from the joint interfaces to the *locations of partial hinges*, as highlighted by red dash lines in Fig. 7. Under large deformations, the rotations mainly occurred at plastic hinges or sections with large cracks, and a large segment of the beam approximately rotated as a rigid body. The shift of plastic hinges from joint interfaces to partial hinge locations suggests that the effective length of beams in rigid body rotation shortened, as illustrated in Fig. 8. That is, for a given MJD, the rotation of the beams of specimen F-PH is greater than that of specimen F-CD. Accordingly, axial tension in beams can be more effectively contributed to sustain vertically applied load, since the vertical projection of axial tension is larger.

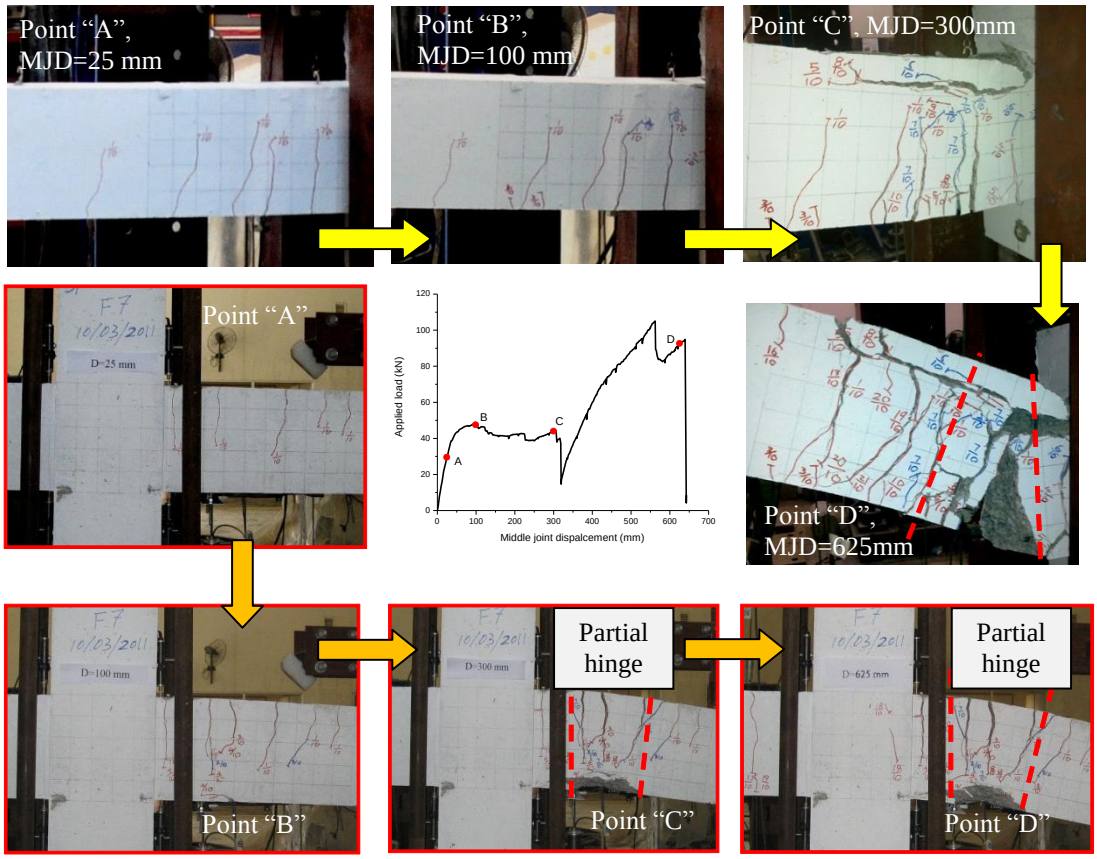

Fig. 7: Failure modes of specimen F-PH

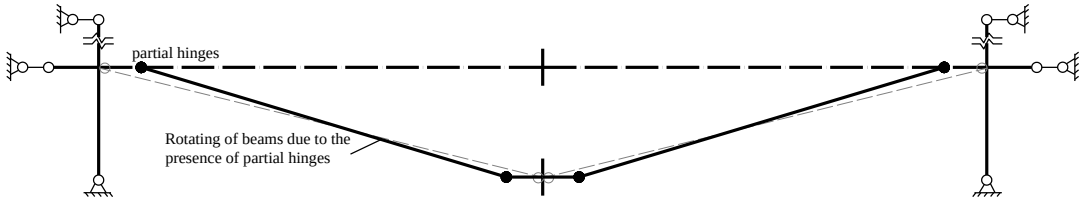

Fig. 8: Effect of partial hinges on beam rotations

3.4 Force transfer mechanism at reinforcement level

Readings of strain gages located in the beam-column joints and the connections provide more insight into force transfer mechanisms in the load-deflection history. Fig. 9(a) shows the layout of strain gages attached onto a top and a bottom bar in the side joint connected to A-Frame. "St" and "Sb" indicates the top and the bottom bar in a side joint, respectively. To investigate the effect of shear force on the strain measurements of a longitudinal bar near the side joint interface, strain gages were attached at both the top and the bottom surfaces of the bar. The label with "A" indicates the strain gage mounted on the bottom surface. For the

bottom bar, all the strain gages were attached onto the side surface of the bar. It was found that shear force slightly affected the strains of bars under tension. Therefore, the strain gages at the same layer near the joint interface were selected to demonstrate the strain distribution of bars. However, some strain gages were spoiled during casting, so their data are not shown.

Hogging moment and axial force were transferred from the two-bay beam to the side joint, resulting in top bars in tension and bottom bars in compression. Fig. 9(b) shows the strain distribution of a top bar in the side joint under different MJDs. It can be seen that the bar tension was significantly reduced only within the joint due to bond stress. However, with increasing MJD, yielding penetration developed quickly. At a MJD of 100 mm, it has advanced around 100 mm from the joint interface to the joint center. The eventual length of bar yielding was around 125 mm (i.e. half joint depth) prior to bar fracture. Fig. 9(c) demonstrates the strain distribution of a bottom bar under different MJDs. Due to bond stress within the joint, the large compressive strain at the joint interface was nearly reduced to zero.

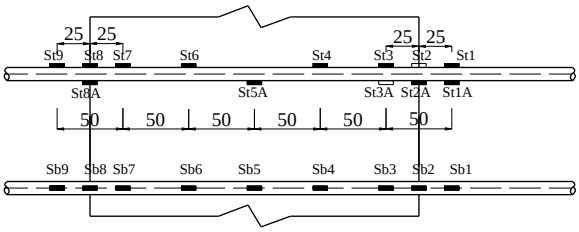

(a) Layout of strain gages (units: mm)

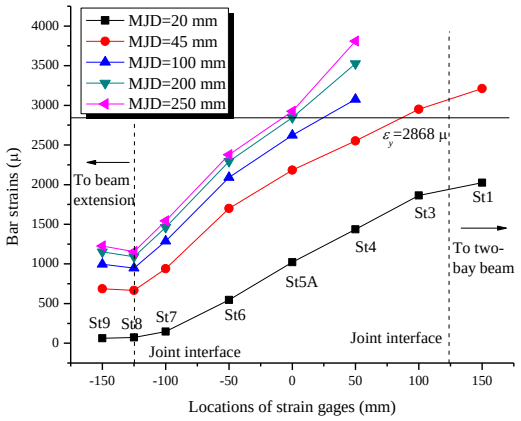

(b) Strain distribution along top bar

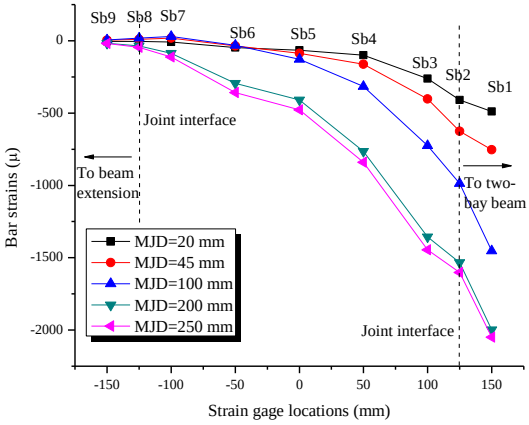

(c) Strain distribution along bottom bar

Fig. 9: Strain distribution over bars in a side joint of F-CD

Fig. 10(a) shows the layout of strain gages for bars in a partial hinge connected to a side joint. Strain gages mounted onto the bent part of the bars are labeled with "X". It can be found that the bent parts were always in tension associated with large tensile strains, such as St3X in Fig. 10(b) and Sb3X in Fig. 10(c). Under hogging moment, the strain at the top bar near the joint interface increased quickly in tension, such as St5 in Fig. 10(b). Despite St3X at 200 mm away from the joint interface (i.e. location of the maximum hogging moment) and close to the geometric center of a beam section, the strain at St3X still increased rapidly. The development of strains at the bent part of bars will be explained later. The strain of top bars at the center of the joint, denoted as St6 in Fig. 10(b), never reached yield strain, indicating that the yielding penetration (or stress level) in the side joint of specimen F-PH is smaller than that in specimen F-CD. Moreover, near the joint interfaces, the compressive strains of bars were very small, not greater than 500μ, such as Sb4 and Sb5 in Fig. 10(c). As a result, no concrete crushing was observed near the joint interface. In a word, the presence of the partial hinge shifts large stress from the joint interface to the partial hinge location.

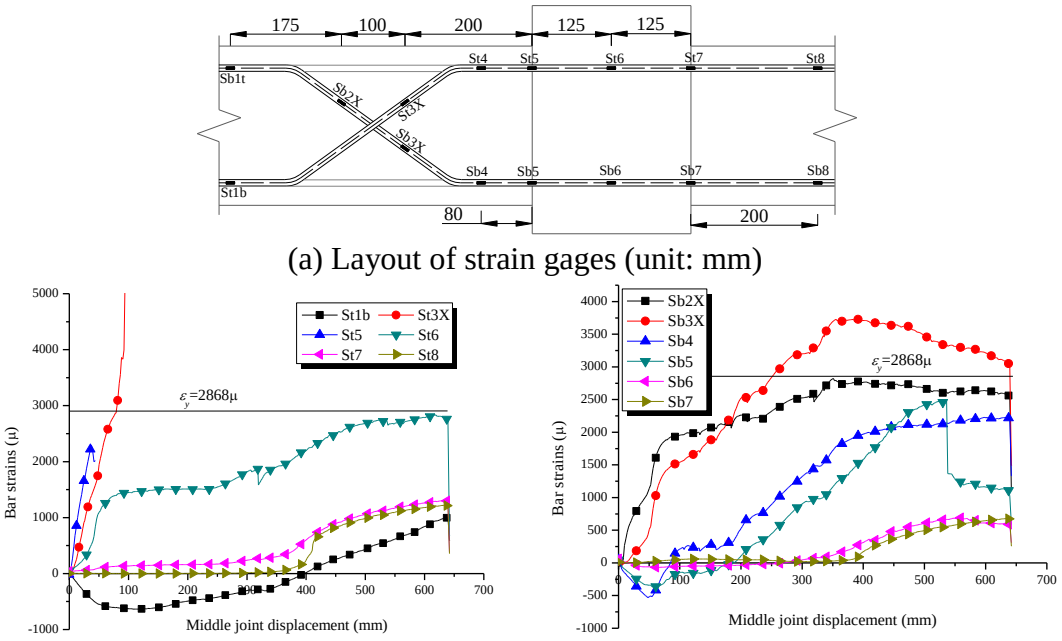

(a) Layout of strain gages (unit: mm)

(b) Bent-down bar

(c) Bent-up bar

Fig. 10: Development of bar strains in a partial hinge adjacent to a side joint

Fig. 11 illustrates the force transfer mechanism within a partial hinge by a "truss analogy". The dash lines in the truss, representing the top and the bottom chords, were analogous to the straight bars, which are 2T13 in the top layer and 2T10 in the bottom layer as shown in Fig. 2(b). Subjected to a combined action of hogging moment and axial force, both the top chord and the inclined members were elongated due to tension whereas the bottom chord was contracted due to compression. This is why the bent parts of the bars were always in tension during the test. The compression of the bottom bars in the partial hinge corresponded to severe crushing of concrete shown in Fig. 7.

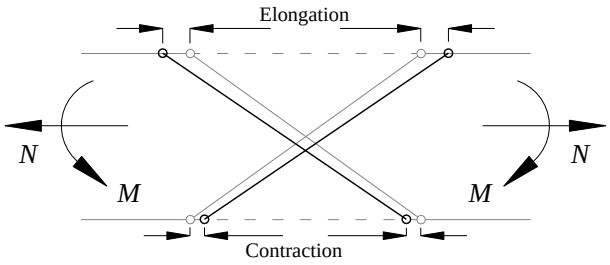

Fig. 11: Force transfer mechanism in partial hinge by truss analysis

4. Discussions

For specimen F-CD, since severe cracks were concentrated at the joint interfaces, the rotation capacity of an RC beam-column connection under large deformations depends on bar slip at the joint interfaces. Moreover, the slip is mainly contributed by plastic elongation of embedded continuous bars within the joints. For example, the slip of a top bar in the side joint of specimen F-CD, as shown in Fig. 9(b), is determined by elongation of the bar with 125 mm long, corresponding to yielding penetration length. In the middle joint of F-CD, the bottom bars were subjected to axial tension at both the joint interfaces. Accordingly, the available bar length for elongation at each side was around 125 mm as well. In addition, the plastic elongation is reduced by bond strength. Large axial compression in columns enhances the bond strength in joints and thus further reduces bar elongation.

For specimen F-PH, the high bar stress level was shifted from joint interfaces to partial hinge locations. The bond strength in beams is smaller than that in joint panels. As a result,

bars in the partial hinges can elongate more easily. As shown in Fig. 7, the large bar stress even induced bond cracks from the middle joint interface to the partial hinge. Moreover, after fracture of top or bottom chord, the beam depth was reduced significantly, increasing rotation capacity. Also, the hinge mechanism per se has a large rotation capacity. As a result, specimen F-PH could proceed to a larger deflection of 562 mm with greater structural resistance.

5. Conclusions

In this paper, the test results of two one-half scaled RC frames subjected to a column removal scenario are demonstrated. The catenary action of specimen F-CD, designed with conventional non-seismic detailing in accordance with ACI 318-05, failed to increase structural resistance beyond compressive arch action (CAA) capacity due to excessive bar fractures near the joint interfaces. On the other hand, catenary action of specimen F-PH, designed with partial hinges in the beams at one beam depth away from the joint interfaces, enhanced its resistance to 2.2 times CAA capacity. The advantages (or reasons) of partial hinge detailing to increase cateanry action resistance of RC frames are as follows:

(1). Partial hinges increases the rotation capacity of beam-column connections;
(2). Partial hinges reduces the effective length of beam segments in rigid rotation, enabling beam axial tension to be more effective to sustain vertical loads (i.e. a larger vertical projection of beam axial tension under a given deflection).

The failure of beam-column connections of specimen F-CD also confirms the concerns in UFC 4-023-03 that the tensile bars in beams may fail to provide tensile forces under large rotations. It is necessary to come up with an approach to assess the rotation capacity of RC beam-column connections under a combined action of bending moment and axial tension.

Acknowledgements

The authors gratefully acknowledge the funding entitled as “Effects of catenary and membrane actions on the collapse mechanisms of RC buildings”, which is provided by Defence Science & Technology Agency, Singapore.

References

[1] Sadek, F., Main, J. A., Lew, H. S., and Bao, Y. H. *Testing and Analysis of Steel and Concrete Beam-Column Assemblies under a Column Removal Scenario*. Journal of Structural Engineering, Vol 137, No. 9, pp. 881-892, 2011.
[2] Sasani, M., Kropelnicki, J. *Progressive collapse analysis of an RC structure*. The Structural Design of Tall and Special Buildings, Vol 17, No. 4, pp. 757-771, 2008.
[3] Yu, J., Tan, K. H. *Experimental and numerical investigation on progressive collapse resistance of reinforced concrete beam column sub-assemblages*. Engineering Structures. 2011(online).
[4] Choi, H., Kim, J. *Progressive collapse-resisting capacity of RC beam–column sub-assemblage*. Magazine of Concrete Research, Vol 63, No. 4, pp. 297-310, 2011.
[5] Su, Y., P., Tian, Y., and Song, X. S. *Progressive collapse resistance of axially-restrained frame beams*. ACI Structural Journal. Vol 106, No. 5, pp. 600-607, 2009.
[6] Yu, J., Tan, K. H. *Structural behavior of reinforced concrete beam column sub-assemblages under a middle column removal scenario*. Journal of Structural Engineering. 2011(submitted).
[7] Yi, W. J., He, Q. F., Xiao, Y., and Kunnath, S, K. *Experimental study on progressive collapse-resistant behavior of reinforced concrete frame structures*. ACI Structural Journal, Vol 105, No. 4, pp. 433-439, 2008.
[8] Yu, J., Tan, K. H. *Experimental study on catenary action of RC beam-column sub-assemblages*. The Third International fib Congress and Exhibition. Gaylord National Resort, Washington, D.C. 2010, Paper #205 in Proceedings Disc.